Journal of the Optical Society of America B
OPTICAL PHYSICS

Plasmonic switches based on subwavelength cavity resonators

Pouya Dastmalchi[1,2] and Georgios Veronis[1,2,*]

[1]School of Electrical Engineering and Computer Science, Louisiana State University, Baton Rouge, Louisiana 70803, USA
[2]Center for Computation and Technology, Louisiana State University, Baton Rouge, Louisiana 70803, USA
*Corresponding author: gveronis@lsu.edu

Received 7 June 2016; revised 25 October 2016; accepted 26 October 2016; posted 26 October 2016 (Doc. ID 267900); published 11 November 2016

We design and optimize highly compact plasmonic switches with high modulation depth and moderate insertion loss, consisting of a metal-dielectric-metal waveguide coupled to a subwavelength cavity resonator. We consider a multisection cavity resonator which comprises multiple sections of varying widths. We find that the optimal structure is a perturbation of the maximum size cavity obtained by reducing the width of the middle section in order to tune the resonant wavelength of the cavity. In addition, the on-resonance modulation depth of the optimized multisection cavity switch is greatly enhanced with respect to a conventional Fabry–Perot cavity switch. We use a single-mode scattering matrix theory to account for the behavior of these systems.

OCIS codes: (250.5403) Plasmonics; (240.6680) Surface plasmons; (130.2790) Guided waves; (130.4815) Optical switching devices.

http://dx.doi.org/10.1364/JOSAB.33.002486

1. INTRODUCTION

Plasmonic waveguide devices could provide an interface between conventional diffraction limited optics and nanoscale electronic and optoelectronic devices [1–6]. One of the main challenges in plasmonics is actively controlling the flow of light in nanoscale plasmonic devices. Active plasmonic devices such as switches and modulators will be critically important for on-chip applications of plasmonics [6–19]. Several different approaches to actively control light in nanoscale plasmonic devices have been explored, including thermally induced changes in the refractive index [8,20–22], direct ultrafast optical excitation of the metal [23], as well as the incorporation of nonlinear [24–26], electro-optic [10,27], and tunable gain [28] and absorbing [29–31] media in plasmonic devices.

When designing compact plasmonic switches, one would like to simultaneously achieve high modulation depth as well as low insertion loss [7,32]. One of the challenges in the design is that in many cases there is a trade-off between the modulation depth and the insertion loss [29]. Another challenge is that for subwavelength active regions the modulation depth is typically low due to the weak light–matter interaction.

In this paper, we design and optimize highly compact plasmonic switches with high modulation depth and moderate insertion loss, consisting of a metal-dielectric-metal (MDM) waveguide coupled to a subwavelength cavity resonator. The structures are filled with an active material with tunable absorption coefficient. The geometrical parameters of the switches are optimized to maximize the modulation depth, subject to the constraint that the insertion loss is less than 3 dB. Using this constrained optimization approach, we can achieve high modulation depth, while ensuring that the insertion loss remains moderate. In order to optimize the cavity shape, we consider for simplicity a multisection cavity switch in which the cavity resonator comprises multiple sections of varying widths. We find that the optimal structure is a perturbation of the maximum size cavity obtained by reducing the width of the middle section. In addition, the on-resonance modulation depth of the optimized multisection cavity switch is greatly enhanced with respect to a conventional Fabry–Perot cavity switch.

The remainder of the paper is organized as follows. The results obtained for the conventional Fabry–Perot cavity switch and the multisection cavity switch structures are presented in Subsections 2.A and 2.B, respectively. Finally, our conclusions are summarized in Section 3.

2. RESULTS

We use the finite-difference frequency-domain (FDFD) method to investigate the properties of the plasmonic switches. This method allows us to directly use experimental data for the frequency-dependent dielectric constant of metals such as silver [33], including both the real and imaginary parts, with no approximation. Perfectly matched layer absorbing boundary conditions are used at all boundaries of the simulation domain [34]. In all cases considered, the widths of the MDM plasmonic waveguides are much smaller than the wavelength, so that only the fundamental TM waveguide mode is propagating.

A. Fabry–Perot Cavity Switch

We first consider a conventional Fabry–Perot cavity switch consisting of a MDM plasmonic waveguide coupled to a MDM cavity resonator formed by two MDM stubs [Fig. 1(a)]. The waveguide and resonator are filled with an active material with refractive index $n = 2.02 + i\kappa$, corresponding to silicon dioxide doped with CdSe quantum dots (QDs) [29,31,35]. The imaginary part of the refractive index κ is tunable. The *on* state of the switch corresponds to the transparent state of the active material ($\kappa = 0$). When κ is changed to $\kappa = 0.05$ in the cavity region (absorbing state of the material), the switch is turned *off*.

In all cases we consider highly compact subwavelength structures with the length and width of the active region limited to less than 250 nm. The cavity length L as well as the stub length d_s are optimized using a genetic global optimization algorithm in combination with FDFD [36] to maximize the modulation depth of the switch, defined as the difference between the transmission in the *on* and *off* states normalized by the transmission in the *on* state $\frac{T(\kappa=0)-T(\kappa=0.05)}{T(\kappa=0)}$, at $\lambda_0 = 1.55$ μm, subject to the constraint that the transmission in the *on* state is $T(\kappa = 0) \geq 0.5$. In other words, we maximize the modulation depth subject to the constraint that the insertion loss, defined as $-10 \log_{10}[T(\kappa = 0)]$, is less than 3 dB. Using this approach, we find that the optimized parameters are $L = 188$ nm and $d_s = 94$ nm, resulting in modulation depth of 0.24 and transmission in the *on* state of 0.51. The transmission spectra in the *on* state $T(\kappa = 0)$ for the optimized switch obtained using this approach are shown in Fig. 1(b). We observe that the optimized conventional Fabry–Perot cavity switch exhibits a resonance at the $\lambda_0 = 1.55$ μm wavelength at which it was optimized. The on-resonance transmission is 0.51, exceeding the 0.5 threshold. However, the modulation depth of the optimized switch at $\lambda_0 = 1.55$ μm is 0.24 [Fig. 1(c)], which is relatively low.

The transmission in the *on* state and modulation depth for the switch, if the metal is assumed to be lossless, are also shown in Figs. 1(b) and 1(c), respectively. We observe that in the absence of loss in the metal, the resonance occurs approximately at the same wavelength as in the lossy case [Fig. 1(b)]. If the metal is lossless, there is no intrinsic loss in the Fabry–Perot cavity. In addition, since the cavity possesses a mirror reflection symmetry with respect to a vertical mirror plane which bisects the middle section of the cavity, the cavity decay rates into the forward and backward waveguides are equal. These conditions lead to complete transmission at resonance in the lossless metal case [37] [Fig. 1(b)]. We also note that in both the lossless and lossy metal cases, there is no reflection at resonance. Thus, the insertion loss at resonance in the lossy case is entirely due to absorption in the cavity. Finally, the modulation depth at resonance is smaller when the loss in the metal is included [Fig. 1(c)], because the field enhancement in the cavity at resonance is smaller in the lossy case.

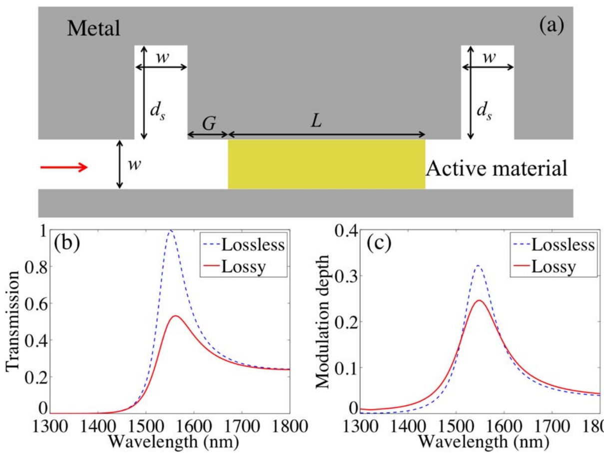

Fig. 1. (a) Schematic of a conventional Fabry–Perot cavity switch consisting of a MDM plasmonic waveguide coupled to a rectangular cavity resonator formed by two MDM stubs. The waveguide and resonator are filled with an active material with refractive index $n = 2.02 + i\kappa$, where κ is tunable. The *on* state of the switch corresponds to $\kappa = 0$. When κ is changed to $\kappa = 0.05$ in the $L \times w$ cavity region, the switch is turned *off*. The arrow indicates the direction of the incident mode. (b) Transmission spectra $T(\kappa = 0)$ for the optimized Fabry–Perot cavity switch of (a) in the *on* state (solid line). Also shown are the transmission spectra if the metal is lossless (dashed line). Results are shown for $w = 50$ nm, $d_s = 94$ nm, $G = 50$ nm, $L = 188$ nm. The metal is silver. (c) Modulation depth as a function of wavelength for the optimized switch of (a) (solid line). Also shown is the modulation depth as a function of wavelength if the metal is lossless (dashed line). All other parameters are as in (b).

B. Multisection Cavity Switch

In an attempt to increase the modulation depth without increasing the insertion loss, we consider a cavity switch as in Fig. 2(a), in which the resonator has an arbitrary shape. Since only the fundamental TM mode is propagating in the MDM waveguide, we can use a single-mode scattering matrix theory to account for the behavior of this system [38]. The complex

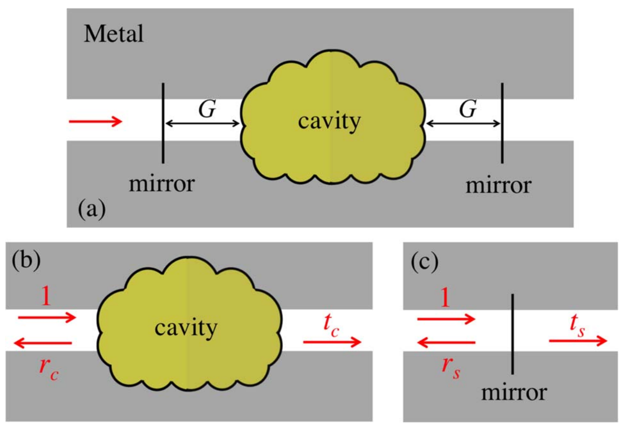

Fig. 2. (a) Schematic of a plasmonic switch consisting of a cavity placed between two partially reflecting elements (black lines). The red arrow indicates the direction of the incident mode. (b) Schematic defining the reflection coefficient r_c, and transmission coefficient t_c when the fundamental TM mode of the MDM waveguide is incident on the cavity. (c) Schematic defining the reflection coefficient r_s, and transmission coefficient t_s when the fundamental TM mode of the MDM waveguide is incident on the partially reflecting element.

magnetic field reflection and transmission coefficients for the cavity (r_c and t_c) and the partially reflecting mirrors (r_s and t_s), when the fundamental waveguide mode is incident on them, are defined as shown in Figs. 2(b) and 2(c), respectively. These coefficients can be numerically extracted using FDFD [38]. The transmission of the switch can then be calculated using scattering matrix theory as [38,39]

$$T = \left| \frac{t_s^2 t_c e^{-2\gamma G}}{1 - 2 r_s r_c e^{-2\gamma G} + (r_s^2 r_c^2 - r_s^2 t_c^2) e^{-4\gamma G}} \right|^2, \tag{1}$$

where γ is the complex propagation constant of the fundamental propagating TM mode in the MDM waveguide, and G is the length of the gap between the mirrors and the cavity [Fig. 2(a)]. In the absence of the cavity ($t_c = 1$, $r_c = 0$), Eq. (1) above reduces to

$$T = \left| \frac{t_s^2 e^{-2\gamma G}}{1 - r_s^2 e^{-4\gamma G}} \right|^2, \tag{2}$$

which is the well-known equation for the transmission of a Fabry–Perot resonator with length $2G$ [40].

In order to optimize the cavity shape, we consider for simplicity a multisection cavity switch in which the resonator cavity comprises multiple sections of varying widths [Fig. 3(a)]. The structure is symmetric with respect to a vertical mirror plane which bisects the middle section of the cavity, and, as in the previous case, the total length and width of the active region are limited to less than 250 nm. As in the conventional Fabry–Perot cavity switch case, the cavity sections widths $d_1, \ldots, d_m$, as well as the stub length d_s are optimized to maximize the modulation depth of the switch, subject to the constraint that the transmission in the *on* state is at least 0.5. Using this approach, we find that the optimized parameters for a multisection cavity with five sections ($m = 3$) are $d_1 = 250$ nm, $d_2 = 250$ nm, $d_3 = 150$ nm, $d_s = 172$ nm. The length of each of the five sections is 50 nm, so that the total length of the active region is 250 nm. We observe that the optimized structure has a relatively simple shape: it can be considered as a perturbation of the 250 nm×250 nm maximum size cavity obtained by reducing the width of the middle section d_3 [Fig. 3(b)]. As in the conventional Fabry–Perot cavity switch case, the optimized multisection cavity switch exhibits a resonance at the 1.55 μm wavelength at which it was optimized, and the on-resonance transmission of 0.51, exceeds the 0.5 threshold [Fig. 3(c)]. In addition, the on-resonance modulation depth of the optimized multisection cavity switch is 0.69 [Fig. 3(d)], and is greatly enhanced with respect to the conventional Fabry–Perot cavity switch [Fig. 1(c)].

As in the conventional Fabry–Perot cavity switch case, we also show the transmission in the *on* state and the modulation depth for the multisection cavity switch, if the metal is assumed to be lossless, in Figs. 3(c) and 3(d), respectively. In the absence of loss in the metal, the resonance occurs approximately at the same wavelength as in the lossy case. Similar to the conventional Fabry–Perot cavity switch, there is complete on-resonance transmission in the lossless metal case, and there is no on-resonance reflection in both the lossless and lossy metal cases, so that the insertion loss at resonance in the lossy case is entirely due to the absorption in the cavity. In addition, the

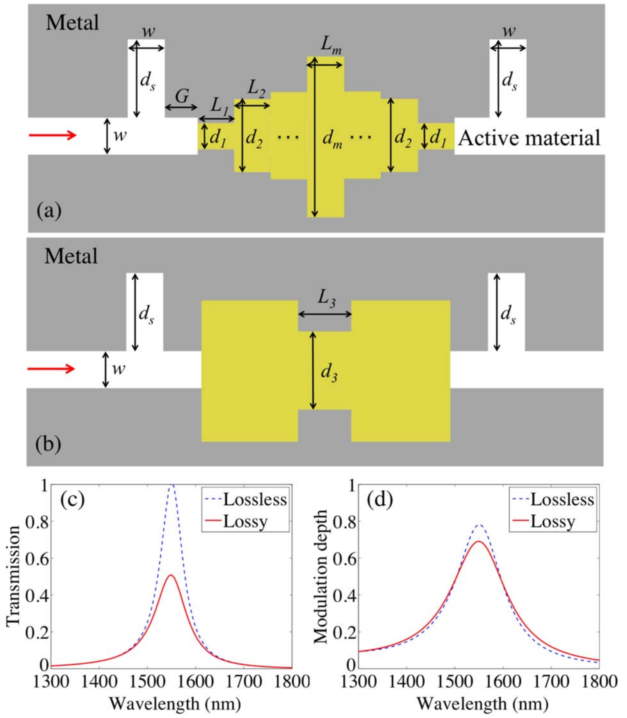

Fig. 3. (a) Schematic of a multisection cavity switch consisting of a MDM plasmonic waveguide coupled to a resonator. The resonator is formed by a cavity comprising multiple sections of varying widths sandwiched between two MDM stubs. The arrow indicates the direction of the incident mode. (b) Schematic of the optimized multisection cavity switch. It can be considered as a perturbation of the maximum size cavity obtained by reducing the width of the middle section d_3. (c) Transmission spectra $T(\kappa = 0)$ for the optimized multisection cavity switch of (a) in the *on* state (solid line). Also shown are the transmission spectra if the metal is lossless (dashed line). Results are shown for $w = 50$ nm, $d_s = 172$ nm, $G = 50$ nm, $d_1 = 250$ nm, $d_2 = 250$ nm, $d_3 = 150$ nm, $L_1 = L_2 = L_3 = 50$ nm. (d) Modulation depth as a function of wavelength for the optimized switch of (a) (solid line). Also shown is the modulation depth as a function of wavelength if the metal is lossless (dashed line). All other parameters are as in (c).

on-resonance modulation depth is slightly smaller when the loss in the metal is included [Fig. 3(d)].

To gain further insight into the properties of the optimized multisection cavity switch, we calculate the transmission in the *on* state and the modulation depth of the switch as a function of the width d_3 and length L_3 of the middle section, and the stub length d_s [Fig. 3(b)].

Figure 4(a) shows that the maximum transmission in the *on* state and maximum modulation depth of the multisection cavity switch are both achieved when the width of the middle section is optimized ($d_3 = 150$ nm). We found that the width of the middle section d_3 is a tuning parameter of the multisection resonator. More specifically, by changing d_3, the resonant wavelength of the cavity can be tuned [Fig. 4(b)]. As d_3 decreases, the resonant wavelength increases. When $d_3 = 150$ nm, the resonant wavelength of the cavity coincides with the operating wavelength of $\lambda_0 = 1.55$ μm [Fig. 4(b)]. Thus, both the transmission in the *on* state and the modulation depth are resonantly enhanced. In Fig. 4(a), in addition to the numerically calculated

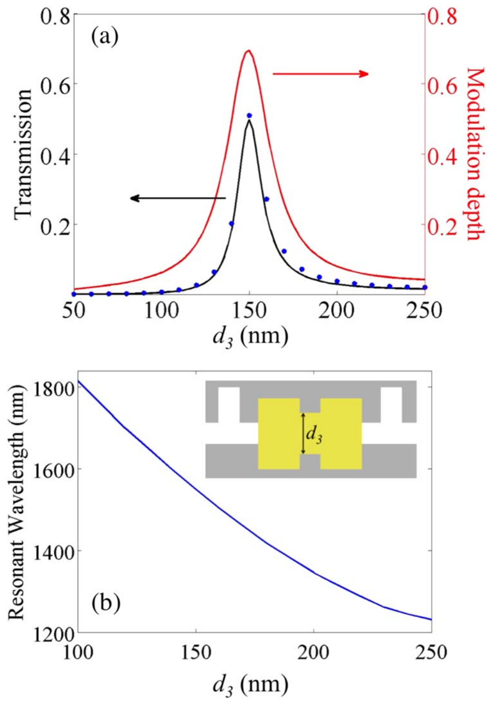

Fig. 4. (a) Transmission in the *on* state (black curve) and modulation depth (red curve) of the optimized multisection cavity switch [shown in the inset of (b)] at $\lambda_0 = 1.55$ μm as a function of the width of the middle section d_3. All other parameters are as in Fig. 3(c). The transmission calculated using scattering matrix theory [Eq. (1)] is also shown (blue dots). (b) Resonant wavelength of the multisection cavity as a function of the width of the middle section d_3. All other parameters are as in Fig. 3(c).

transmission in the *on* state obtained with FDFD, we also show the transmission calculated using scattering matrix theory [Eq. (1)]. We observe that there is excellent agreement between the scattering matrix theory results and the exact results obtained using FDFD, confirming the validity of scattering matrix theory in describing the properties of the multisection cavity switches.

In Fig. 5 we show the transmission in the *on* state and the modulation depth of the switch as a function of the width d_3 and length L_3 of the middle section. We observe that both the transmission and the modulation depth are highly sensitive to the width d_3 of the middle section. This is due to the fact that, as mentioned above, the width of the middle section tunes the resonant wavelength of the cavity. In contrast, the transmission and the modulation depth are not particularly sensitive to the length L_3 of the middle section (Fig. 5). The dependence of the transmission and modulation depth of the switch on the width and length of the middle section of the cavity are reminiscent of the dependence of the modal properties of a plasmonic slot waveguide on the width and length of its slot [41]. The modal properties are largely determined by the slot width, while they are essentially insensitive to the slot length for sufficiently large length [41].

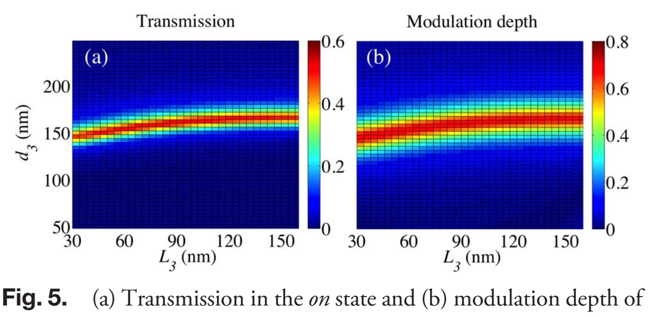

Fig. 5. (a) Transmission in the *on* state and (b) modulation depth of the multisection cavity switch as a function of the width d_3 and length L_3 of the middle section of the cavity at $\lambda_0 = 1.55$ μm. All other parameters are as in Fig. 3(c).

As mentioned above, when the switch is turned *off*, the imaginary part κ of the refractive index $n = 2.02 + i\kappa$ of the active material filling the cavity region is changed from $\kappa = 0$ to $\kappa = 0.05$. As a result, when the switch is turned *off*, the imaginary part of the dielectric constant of the active material changes, while the change in its real part is very small. Thus, the modulation depth of the switches is mostly associated with the sensitivity of their transmission to the imaginary part of the dielectric constant of the active material ε_{r_i} [42–45]. To confirm this, we calculate the sensitivity of the transmission of the multisection cavity switch to the imaginary part of the dielectric constant of the active material [Fig. 6(a)]. We indeed observe that, when the structure is on resonance, the normalized sensitivity of the transmission to the imaginary part of the dielectric constant of the active material, $T^{-1}\frac{\partial T}{\partial \varepsilon_{r_i}}$, and therefore the modulation depth are resonantly enhanced [Fig. 6(a)].

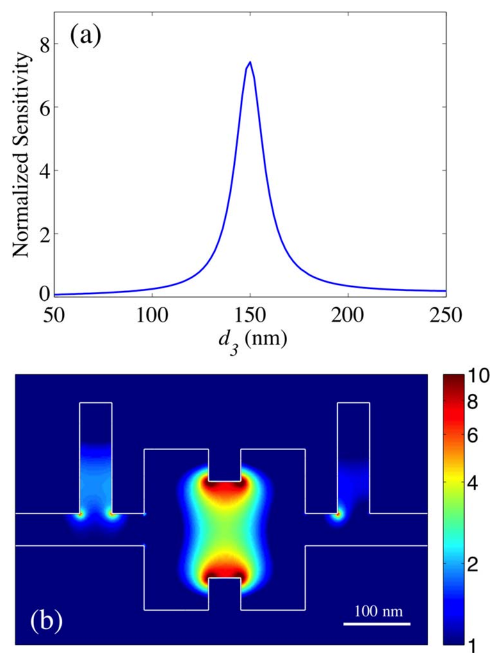

Fig. 6. (a) Normalized sensitivity of the transmission of the multisection cavity switch to the imaginary part of the dielectric constant of the active material, $T^{-1}\frac{\partial T}{\partial \varepsilon_{r_i}}$, at $\lambda_0 = 1.55$ μm as a function of the width of the middle section d_3. All other parameters are as in Fig. 3(c). (b) Profile of the electric field amplitude for the optimized switch of Fig. 3(b) at $\lambda_0 = 1.55$ μm, normalized with respect to the maximum field amplitude of the incident MDM waveguide mode. All other parameters are as in Fig. 3(c).

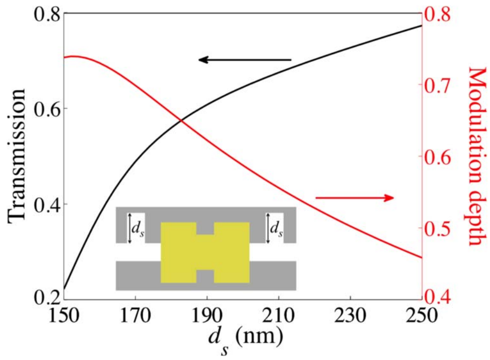

Fig. 7. Transmission in the *on* state (black curve) and modulation depth (red curve) of the optimized multisection cavity switch (shown in the inset) as a function of the length of the MDM stubs d_s at $\lambda_0 = 1.55$ μm. All other parameters are as in Fig. 3(c).

The sensitivity of the transmission to the imaginary part of the dielectric constant of the active material is in turn directly related to the electric field intensity in the cavity region [42–45]. More specifically, we found that the sensitivity of the optimized multisection cavity switch [Fig. 3(a)] is greatly enhanced compared to the optimized conventional Fabry–Perot cavity switch [Fig. 1(a)] due to the great enhancement of the electric field intensity in the cavity region. The profile of the electric field amplitude for the optimized multisection cavity switch is shown in Fig. 6(b). The maximum electric field intensity in the cavity filled with the active material is around the tips of its middle section. The enhanced field intensity in the cavity increases the interaction of light with matter, and the absorption in the *off* state is therefore enhanced.

In Fig. 7 we show the transmission in the *on* state and the modulation depth of the switch as a function of the stub length d_s. We observe that there is a trade-off between the transmission and the modulation depth when the stub length d_s is varying. We found that, as d_s increases, the stub transmittance increases, while the stub reflectance decreases. As a result, as the stub length d_s increases, the transmission in the *on* state of the switch increases (Fig. 7). On the other hand, the optimum light–matter interaction in the cavity, and therefore the optimum modulation depth, occur when the energy density in the cavity is maximized [7]. In addition, to maximize the energy density in the cavity, high stub reflectance is required [7]. Thus, since, as the stub length d_s increases, the stub reflectance decreases, the modulation depth of the switch also decreases (Fig. 7). As mentioned above, the optimized stub length was found to be $d_s = 172$ nm. As can be seen in Fig. 7, the choice of this parameter is dictated by the optimization constraint that the transmission in the *on* state must be at least 0.5. Reducing the stub length d_s would result in increased modulation depth. This, however, would be at the cost of decreased transmission in the *on* state (Fig. 7).

3. CONCLUSIONS

In this paper, we introduced compact absorption switches consisting of a plasmonic MDM waveguide coupled to a multisection cavity. We considered highly compact structures with subwavelength active region. The structures are filled with an active material with tunable absorption coefficient. The geometrical parameters of the switches were optimized to maximize the modulation depth, subject to the constraint that the insertion loss is less than 3 dB.

We first considered a conventional Fabry–Perot cavity switch consisting of a MDM plasmonic waveguide coupled to a MDM cavity resonator formed by two MDM stubs. We found that the optimized conventional Fabry–Perot cavity switch exhibits a resonance at the wavelength at which it was optimized. However, the modulation depth of the optimized switch is relatively low.

In an attempt to increase the modulation depth without increasing the insertion loss, we then considered a cavity switch in which the resonator has an arbitrary shape. We used a single-mode scattering matrix theory to account for the behavior of this system. In order to optimize the cavity shape, we considered for simplicity a multisection cavity switch in which the resonator cavity comprises multiple sections of varying widths. In this case, we found that the optimized structure is a perturbation of the maximum size cavity obtained by reducing the width of the middle section. In addition, the on-resonance modulation depth of the optimized multisection cavity switch is greatly enhanced with respect to the conventional Fabry–Perot cavity switch.

We found that the width of the middle section can be used to tune the resonant wavelength of the multisection resonator. For the optimized structure the resonant wavelength of the cavity coincides with the operating wavelength, so that both the transmission in the *on* state and the modulation depth are resonantly enhanced. In addition, the modulation depth of the switches is directly associated with the sensitivity of their transmission to the imaginary part of the dielectric constant of the active material, which is in turn directly related to the electric field intensity in the cavity region. We found that the sensitivity of the optimized multisection cavity switch is greatly enhanced compared to the optimized conventional Fabry–Perot cavity switch due to the great enhancement of the electric field intensity in the cavity region. We also found that there is a trade-off between the transmission in the *on* state and the modulation depth when the length of the stubs is varying. The choice of the stub length is dictated by the optimization constraint that the insertion loss must be less than 3 dB.

As final remarks, we note that similar highly compact plasmonic switches based on subwavelength cavity resonators could also be implemented using other plasmonic two-conductor waveguides, such as three-dimensional plasmonic coaxial waveguides [46,47]. We also note that there are some analogies between the enhancement of modulation depth in the proposed plasmonic switches based on subwavelength cavity resonators, and the enhancement of transmission through C-shaped nanoapertures. In C-shaped apertures the modification of the aperture shape increases the cutoff wavelength of the relevant waveguide mode leading to increased transmission [48,49]. Similarly, in the subwavelength cavity resonators considered here, reducing the width of the middle section increases the resonant wavelength of the cavity leading to resonant enhancement of the modulation depth.

Finally, we note that the switching time of the active material considered in this paper (QD-doped silicon dioxide) is limited by the QD-exciton recombination lifetime, which is of the order of 40 ns [31,35]. In addition to QD-doped silicon dioxide, several other materials with tunable absorption coefficient can be used, such as photochromic molecules [30], multiple quantum well structures [50,51], and heavily doped silicon [52]. The use of heavily doped silicon could lead to switching times of less than 1 ps [52].

Funding. National Science Foundation (NSF) (1102301, 1254934).

REFERENCES

1. S. A. Maier, *Plasmonics: Fundamentals and Applications* (Springer, 2007).
2. H. A. Atwater, "The promise of plasmonics," Sci. Am. **296**, 56–62 (2007).
3. D. K. Gramotnev and S. I. Bozhevolnyi, "Plasmonics beyond the diffraction limit," Nat. Photonics **4**, 83–91 (2010).
4. J. A. Schuller, E. S. Barnard, W. Cai, Y. C. Jun, J. S. White, and M. L. Brongersma, "Plasmonics for extreme light concentration and manipulation," Nat. Mater. **9**, 193–204 (2010).
5. G. Veronis and S. Fan, "Bends and splitters in subwavelength metal-dielectric-metal plasmonic waveguides," Appl. Phys. Lett. **87**, 131102 (2005).
6. N. Kinsey, M. Ferrera, V. Shalaev, and A. Boltasseva, "Examining nanophotonics for integrated hybrid systems: a review of plasmonic interconnects and modulators using traditional and alternative materials," J. Opt. Soc. Am. B **32**, 121–142 (2015).
7. W. Cai, J. S. White, and M. L. Brongersma, "Compact, high-speed and power-efficient electrooptic plasmonic modulators," Nano Lett. **9**, 4403–4411 (2009).
8. A. V. Krasavin and N. Zheludev, "Active plasmonics: controlling signals in Au/Ga waveguide using nanoscale structural transformations," Appl. Phys. Lett. **84**, 1416–1418 (2004).
9. G. Wurtz, R. Pollard, and A. Zayats, "Optical bistability in nonlinear surface-plasmon polaritonic crystals," Phys. Rev. Lett. **97**, 057402 (2006).
10. M. J. Dicken, L. A. Sweatlock, D. Pacifici, H. J. Lezec, K. Bhattacharya, and H. A. Atwater, "Electrooptic modulation in thin film barium titanate plasmonic interferometers," Nano Lett. **8**, 4048–4052 (2008).
11. V. V. Temnov, G. Armelles, U. Woggon, D. Guzatov, A. Cebollada, A. Garcia-Martin, J.-M. Garcia-Martin, T. Thomay, A. Leitenstorfer, and R. Bratschitsch, "Active magneto-plasmonics in hybrid metal-ferromagnet structures," Nat. Photonics **4**, 107–111 (2010).
12. S. Fan, "Nanophotonics: magnet-controlled plasmons," Nat. Photonics **4**, 76–77 (2010).
13. V. J. Sorger, N. D. Lanzillotti-Kimura, R.-M. Ma, and X. Zhang, "Ultra-compact silicon nanophotonic modulator with broadband response," Nanophotonics **1**, 17–22 (2012).
14. A. Melikyan, L. Alloatti, A. Muslija, D. Hillerkuss, P. C. Schindler, J. Li, R. Palmer, D. Korn, S. Muehlbrandt, D. Van Thourhout, B. Chen, R. Dinu, M. Sommer, C. Koos, M. Kohl, W. Freude, and J. Leuthold, "High-speed plasmonic phase modulators," Nat. Photonics **8**, 229–233 (2014).
15. H. W. Lee, G. Papadakis, S. P. Burgos, K. Chander, A. Kriesch, R. Pala, U. Peschel, and H. A. Atwater, "Nanoscale conducting oxide plasMOStor," Nano Lett. **14**, 6463–6468 (2014).
16. A. Emboras, C. Hoessbacher, C. Haffner, W. Heni, U. Koch, P. Ma, Y. Fedoryshyn, J. Niegemann, C. Hafner, and J. Leuthold, "Electrically controlled plasmonic switches and modulators," IEEE J. Sel. Top. Quantum Electron. **21**, 276–283 (2015).
17. V. E. Babicheva, A. Boltasseva, and A. V. Lavrinenko, "Transparent conducting oxides for electro-optical plasmonic modulators," Nanophotonics **4**, 165–185 (2015).
18. A. Haddadpour and Y. Yi, "Metallic nanoparticle on micro ring resonator for bio optical detection and sensing," Biomed. Opt. Express **1**, 378–384 (2010).
19. A. E. Cetin, A. Mertiri, M. Huang, S. Erramilli, and H. Altug, "Thermal tuning of surface plasmon polaritons using liquid crystals," Adv. Opt. Mater. **1**, 915–920 (2013).
20. T. Nikolajsen, K. Leosson, and S. I. Bozhevolnyi, "Surface plasmon polariton based modulators and switches operating at telecom wavelengths," Appl. Phys. Lett. **85**, 5833–5835 (2004).
21. A. Lereu, A. Passian, J. Goudonnet, T. Thundat, and T. Ferrell, "Optical modulation processes in thin films based on thermal effects of surface plasmons," Appl. Phys. Lett. **86**, 154101 (2005).
22. J. Gosciniak, S. I. Bozhevolnyi, T. B. Andersen, V. S. Volkov, J. Kjelstrup-Hansen, L. Markey, and A. Dereux, "Thermo-optic control of dielectric-loaded plasmonic waveguide components," Opt. Express **18**, 1207–1216 (2010).
23. K. F. MacDonald, Z. L. Sámson, M. I. Stockman, and N. I. Zheludev, "Ultrafast active plasmonics," Nat. Photonics **3**, 55–58 (2009).
24. G. A. Wurtz and A. V. Zayats, "Nonlinear surface plasmon polaritonic crystals," Laser Photonics Rev. **2**, 125–135 (2008).
25. C. Min, P. Wang, C. Chen, Y. Deng, Y. Lu, H. Ming, T. Ning, Y. Zhou, and G. Yang, "All-optical switching in subwavelength metallic grating structure containing nonlinear optical materials," Opt. Lett. **33**, 869–871 (2008).
26. N. Nozhat and N. Granpayeh, "All-optical logic gates based on nonlinear plasmonic ring resonators," Appl. Opt. **54**, 7944–7948 (2015).
27. W. Dickson, G. A. Wurtz, P. R. Evans, R. J. Pollard, and A. V. Zayats, "Electronically controlled surface plasmon dispersion and optical transmission through metallic hole arrays using liquid crystal," Nano Lett. **8**, 281–286 (2008).
28. Z. Yu, G. Veronis, S. Fan, and M. L. Brongersma, "Gain-induced switching in metal-dielectric-metal plasmonic waveguides," Appl. Phys. Lett. **92**, 041117 (2008).
29. C. Min and G. Veronis, "Absorption switches in metal-dielectric-metal plasmonic waveguides," Opt. Express **17**, 10757–10766 (2009).
30. R. A. Pala, K. T. Shimizu, N. A. Melosh, and M. L. Brongersma, "A nonvolatile plasmonic switch employing photochromic molecules," Nano Lett. **8**, 1506–1510 (2008).
31. D. Pacifici, H. J. Lezec, and H. A. Atwater, "All-optical modulation by plasmonic excitation of CdSe quantum dots," Nat. Photonics **1**, 402–406 (2007).
32. M. Bahramipanah, S. Dutta-Gupta, B. Abasahl, and O. J. Martin, "Cavity-coupled plasmonic device with enhanced sensitivity and figure-of-merit," ACS Nano **9**, 7621–7633 (2015).
33. E. D. Palik, *Handbook of Optical Constants of Solids* (Academic, 1985).
34. J. Jin, *The Finite Element Method in Electromagnetics* (Wiley, 2002).
35. D. Pacifici, H. J. Lezec, L. A. Sweatlock, C. D. Ruiter, V. Ferry, and H. A. Atwater, "All-optical plasmonic modulators and interconnects," in *Plasmonic Nanoguides and Circuits*, S. I. Bozhevolnyi, ed. (World Scientific, 2009).
36. G. Veronis and S. Fan, "Theoretical investigation of compact couplers between dielectric slab waveguides and two-dimensional metal-dielectric-metal plasmonic waveguides," Opt. Express **15**, 1211–1221 (2007).
37. Y. Xu, Y. Li, R. K. Lee, and A. Yariv, "Scattering-theory analysis of waveguide-resonator coupling," Phys. Rev. E **62**, 7389–7404 (2000).
38. S. E. Kocabas, G. Veronis, D. A. B. Miller, and S. Fan, "Transmission line and equivalent circuit models for plasmonic waveguide components," IEEE J. Sel. Top. Quantum Electron. **14**, 1462–1472 (2008).
39. Y. Huang, C. Min, and G. Veronis, "Subwavelength slow-light waveguides based on a plasmonic analogue of electromagnetically induced transparency," Appl. Phys. Lett. **99**, 143117 (2011).
40. N. Hodgson and H. Weber, *Laser Resonators and Beam Propagation* (Springer, 2005).
41. G. Veronis and S. Fan, "Modes of subwavelength plasmonic slot waveguides," J. Lightwave Technol. **25**, 2511–2521 (2007).
42. G. Veronis, R. W. Dutton, and S. Fan, "Method for sensitivity analysis of photonic crystal devices," Opt. Lett. **29**, 2288–2290 (2004).
43. R. F. Harrington, *Time-Harmonic Electromagnetic Fields* (Wiley-IEEE, 2001).

44. A. Raman and S. Fan, “Perturbation theory for plasmonic modulation and sensing,” Phys. Rev. B **83**, 205131 (2011).
45. P. Berini, “Bulk and surface sensitivities of surface plasmon waveguides,” New J. Phys. **10**, 105010 (2008).
46. W. Shin, W. Cai, P. B. Catrysse, G. Veronis, M. L. Brongersma, and S. Fan, “Broadband sharp 90-degree bends and T-splitters in plasmonic coaxial waveguides,” Nano Lett. **13**, 4753–4758 (2013).
47. A. Mahigir, P. Dastmalchi, W. Shin, S. Fan, and G. Veronis, “Plasmonic coaxial waveguide-cavity devices,” Opt. Express **23**, 20549–20562 (2015).
48. X. Shi and L. Hesselink, “Mechanisms for enhancing power throughput from planar nano-apertures for near-field optical data storage,” Jpn. J. Appl. Phys. **41**, 1632–1635 (2002).
49. X. Shi, L. Hesselink, and R. L. Thornton, “Ultrahigh light transmission through a C-shaped nanoaperture,” Opt. Lett. **28**, 1320–1322 (2003).
50. I. Bar-Joseph, C. Klingshirn, D. A. B. Miller, D. S. Chemla, U. Koren, and B. I. Miller, “Quantum-confined Stark effect in InGaAs/InP quantum wells grown by organometallic vapor phase epitaxy,” Appl. Phys. Lett. **50**, 1010–1012 (1987).
51. Y. H. Kuo, Y. K. Lee, Y. Ge, S. Ren, J. E. Roth, T. I. Kamins, D. A. B. Miller, and J. S. Harris, “Strong quantum-confined Stark effect in germanium quantum-well structures on silicon,” Nature **437**, 1334–1336 (2005).
52. S. Sandhu, M. L. Povinelli, and S. Fan, “Stopping and time reversing a light pulse using dynamic loss tuning of coupled-resonator delay lines,” Opt. Lett. **32**, 3333–3335 (2007).